Trace gas monitoring with infrared laser-based detection schemes

Appl. Phys. B 90, 289–300 (2008)
DOI: 10.1007/s00340-007-2875-4

Applied Physics B
Lasers and Optics

M.W. SIGRIST✉
R. BARTLOME
D. MARINOV
J.M. REY
D.E. VOGLER*
H. WÄCHTER

Trace gas monitoring with infrared laser-based detection schemes

ETH Zurich, Institute for Quantum Electronics, Laser Spectroscopy and Sensing Lab, Schafmattstrasse 16, 8093 Zürich, Switzerland

Received: 8 October 2007
Published online: 13 December 2007 • © Springer-Verlag 2007

ABSTRACT The success of laser-based trace gas sensing techniques crucially depends on the availability and performance of tunable laser sources combined with appropriate detection schemes. Besides near-infrared diode lasers, continuously tunable midinfrared quantum cascade lasers and nonlinear optical laser sources are preferentially employed today. Detection schemes are based on sensitive absorption measurements and comprise direct absorption in multi-pass cells as well as photoacoustic and cavity ringdown techniques in various configurations. We illustrate the performance of several systems implemented in our laboratory. These include time-resolved multicomponent traffic emission measurements with a mobile CO_2-laser photoacoustic system, a diode-laser based cavity ringdown device for measurements of impurities in industrial process control, isotope ratio measurements with a difference frequency (DFG) laser source combined with balanced path length detection, detection of methylamines for breath analysis with both a near-IR diode laser and a DFG source, and finally, acetone measurements with a heatable multipass cell intended for vapor phase studies on doping agents in urine samples.

PACS 33.20.Ea; 42.62.Fi; 42.72.Ai; 87.64.km; 92.60.Sz

1 Introduction: Trace gas sensing

Trace gases play a key role in various areas such as air pollution, climate research, industrial process control, agriculture, food industry, volcanology, workplace safety and medical diagnostics. There exist numerous gas sensing devices based on different detection principles like gas chromatography (GC), mass spectrometry (MS) or combinations of the two (GC-MS), chemiluminescence, Fourier transform infrared spectroscopy (FTIR), electrochemical sensors, colorimetry, etc. In recent years, laser-spectroscopic sensing devices have attracted a lot of interest (see e.g., [1]) as they enable high detection sensitivity (down to sub-ppb concentrations) and selectivity (including differentiation between isotopomers and isomers), multicomponent capability and large dynamic range (several orders of magnitude in concentration), and generally neither sample-preparation nor -preconcentration are required. However, the laser source characteristics in terms of available wavelengths, tunability, linewidth, power, operation temperature, etc., as well as the combination with appropriate sensitive detection schemes are crucial for the success of laser-based sensing. Table 1 lists the main sensing requirements and the corresponding approaches using laser-based methods. Ideally, one system can fulfill all requirements. The combination of broad continuous tuning with a narrow linewidth and a certain power level favors laser-based systems.

Sensor requirement	Approach
High sensitivity (ppb to sub-ppb)	Strong fundamental absorption lines in the mid-IR, lower sensitivity in near-IR
High selectivity (including isotopes)	Narrow laser linewidth, eventually reduced gas pressure
Multi-component capability	Broad, preferentially continuous tuning range
Large dynamic range	Balanced absorption pathlength selection of weaker absorption lines for higher concentrations and vice versa
Good time resolution	Neither sample preparation nor pretreatment, preconcentration, etc. Fast accessibility of wavelength of interest
Field capability	Room temperature operation, compact and robust set-up

TABLE 1 Trace gas sensor requirements with corresponding approach for laser-based detection system

2 Laser sources

Tunable near-infrared (near-IR) lasers are readily available, notably diode lasers equipped with an external cavity. These external cavity III-V diode lasers (ECDLs) represent excellent sources in terms of availability, compactness, robustness and tuning characteristics. They are operated at room temperature, yield narrow linewidths and continuous-wave (cw) powers at a level of several mW. Available wavelengths range from the visible to typically ca. 2 μm. Depending on the center wavelength, tuning across some tens of nm is feasible.

✉ Fax: +41-44-633 1230, E-mail: sigristm@phys.ethz.ch
*Now with Leister Process Technologies, Riedstrasse, 6060 Sarnen, Switzerland

The near-IR range is of interest for detecting molecules at higher concentrations, typically in the ppm-range or higher, by sensing molecular absorption overtones or combination bands. The near-IR absorption strengths are typically 100 times weaker than the fundamental absorptions in the mid-IR, but often favorable for simple systems and/or measurements at higher gas concentrations. Ultimate sensitivity, however, requires mid-IR wavelengths where characteristic molecular fundamental absorptions are present, also known as fingerprint region. Hence, emphasis is placed on lasers with emissions in the range between ca. 3 and 15 μm, with emphasis in the 3–4 μm region where the C−H-stretch vibration occurs, common to all hydrocarbons. Available tunable mid-IR sources include CO_2-lasers, color center lasers, solid state lasers, III-V diode lasers and IV-VI lead salt diode lasers, quantum cascade lasers, and nonlinear optical systems. CO_2 lasers emit rather high powers, but enable only discrete wavelength tuning (line-tuning) in the 9–11 μm range with an extension to the 4.5–5.5 μm range (second harmonic generation of CO_2 laser radiation [2]). Continuous tuning of CO_2 lasers is feasible at high gas pressures of approximately 10 bars, yet only pulsed [3]. Color center lasers are hardly used for trace gas sensing [4] as they do not operate in the range beyond approximately 3 μm and generally require a strong pump laser and often cryogenic cooling for the alkali halide crystal containing the color centers. Solid state lasers with emissions exceeding 3 μm are rare. For example, a fiber-laser pumped Cr^{2+}:ZnSe laser exhibits a broad tuning range from 2.2 to 3.1 μm [5] at a cw power of 1 W, or a Fe^{2+}:ZnSe laser emitting between 3.9 and 4.5 μm [6] are mentioned here. While the first device operates at room temperature, the latter needs cryogenic cooling and only runs in pulsed mode. The emission of fiber lasers, e.g., erbium-doped ZBLAN, can be tuned by > 100 nm, but ends around 2.7 μm.

The wavelength range of III-V diode lasers is extended by using GaSb-based materials instead of GaAs or InP. As an example, such lasers with cw operation at room temperature and current and/or temperature tuning around 2.74 μm are commercially available and even longer wavelengths have been reported with interband cascade Sb-based diode lasers (ICL) [7]. Unlike quantum cascade lasers (QCLs, see below), these lasers use transitions between conduction band and valence, band but similar to QCLs, injected electrons are used several times via a cascade structure for the generation of photons, thereby considerably reducing the threshold current density. CW operation at wavelengths around 3.3 μm has recently been achieved with thermoelectric instead of the previous cryogenic cooling [8] and emission beyond 5 μm was realized at cryogenic temperatures of ≤ 163 K for cw and ≤ 240 K for pulsed operation [9]. However, the tuning by current and/or temperature is rather small and wavelength coverage is limited.

An alternative are IV-VI lead salt diode lasers [10, 11]. Depending on the material composition their tunability ranges from approximately 3 μm to 32 μm. Coarse wavelength tuning is achieved by temperature, and fine tuning is achieved by current. The mode-hop free tuning range is typically only 1 cm^{-1}. The drawbacks are the required cryogenic cooling and a rather low power of typically 0.1 mW. More recently, optically pumped lead salt diode lasers have been realized [12, 13].

Quantum cascade lasers (QCLs), introduced in 1994 [14], are semiconductor lasers using transitions within the conduction band. Hence, the wavelength can be tailored by the thickness of the layer rather than being determined by the bandgap. Today, a whole variety of QCLs are commercially available, including pulsed and cw devices with DFG structure, cryogenic or thermoelectric cooling or room temperature. The tuning is typically done by temperature tuning and reaches several cm^{-1}. Today, cw powers of QCLs are typically in the range of several mW with powers > 100 mW being reported [15, 16]. Most recently, external cavity QCLs have been realized [17, 18] which extend the tuning range to typically ±5% of the center wavelength. QCL wavelengths now extend from ca. 4 to beyond 24 μm with devices operating also in the THz region. The wavelength coverage and tuning capabilities, though, are still limited, particularly in the important 3–4 μm range. Nevertheless, QCLs certainly represent very promising sources for gas sensing applications. They are discussed in other papers – notably by Kosterev et al. – in this special issue.

A final option of tunable mid-IR lasers are sources based on nonlinear optical processes. They comprise optical parametric oscillators (OPOs) [19, 20] and difference frequency generation (DFG) [21, 22] devices. Both are room-temperature systems yielding broad tuning ranges often exceeding 100 cm^{-1}. Depending on the nonlinear medium, any wavelength in the 3–15 μm range can be accessed. An often used nonlinear material is periodically poled $LiNbO_3$ called PPLN. It enables tuning in the important 3–4.5 μm range. Many configurations of such systems have been introduced and some commercial apparatuses exist. The drawback of these systems is the rather costly set-up with two primary sources (for DFG), a strong pump laser (for OPO) and an appropriate nonlinear crystal. While the cw power levels are typically in the μW to mW range for DFG systems, high powers even above 2 W are achieved with OPOs.

An important aspect of all sources concerns the linewidth which essentially determines the achievable selectivity, e.g., in multi-component gas mixtures or in isotope-selective studies. In this respect, cw sources are preferred as linewidths of MHz can typically be achieved in a straightforward manner. There is certainly still a need for the further development of tunable mid-IR lasers, as the ideal source does not yet exist. Table 2 summarizes the main characteristics of today's tunable mid-IR lasers. As the ideal source meeting all requirements does not exist, a good compromise can usually be found.

3 Detection schemes

The detection methods for trace gas sensing are typically based on sensitive absorption measurements. These include direct absorption, photoacoustic or cavity ring-down spectroscopy. To enhance the sensitivity in direct absorption, the absorption path length is increased by using multipass cells, mostly of White [23] or Herriott [24] type featuring total path lengths of tens of meters. Furthermore, wavelength modulation (WM) and detection at the first or second

Laser	Wavelength [μm]	Tuning Characteristics	Power	Operation
CO_2	9 to 11	only line tunable	Watts	RT
Sb-based interband cascade	2 to 4.5	few nm	> 10 mW	RT
Lead salt diode	4 to 32	$\sim$ cm^{-1} mode hop free	> 0.1 mW	Cryo
QCL	4 to >24, THz	cm^{-1} to > 100 cm^{-1}	mW to W	Cryo/TE/RT
Solid State[a]	2.2 to 3.1 (3.9 to 4.5)	0.5 to 1 μm	1 W cw (pulsed)	RT (Cryo)
Fiber laser[b]	~2.7	> 100 nm	Watts	RT
OPO[c]	3 to 16	~ μm	> 1 W	RT
DFG[c]	3 to 16	~ μm	μW–mW	RT

[a] Examples: Cr^{2+}:ZnSe laser (Fe^{2+}:ZnSe laser), etc.
[b] Example: Erbium-doped ZBLAN
[c] Examples: PPLN (periodically poled lithium niobate, eventually with waveguide), $AgGaSe_2$, $LiInS_2$, $LiInSe_2$, etc.

TABLE 2 Tunable mid-IR laser sources with main characteristics, RT: room temperature, Cryo: liquid nitrogen cooling, TE: thermoelectric cooling, OPO: optical parametric oscillator, DFG: difference frequency generation

harmonic may be employed. With such configurations, a minimum detectable absorption coefficient (detection sensitivity) of 10^{-7} cm^{-1}Hz$^{-1/2}$ can typically be achieved. This enables monitoring of ppb gas concentrations if measurements are performed at the fundamental absorption wavelengths. Provided that sensitive IR detectors like thermoelectrically cooled or room-temperature photoconductive detectors or even liquid nitrogen cooled mercury cadmium telluride (MCT) detectors are employed, direct absorption measurements with multipass cells are feasible even at low laser power levels of μW.

An alternative approach uses the photoacoustic (PA) effect originally introduced in 1880 [25] and experiencing a renaissance with the advent of lasers. Various types of PA cell designs have been developed [26, 27], including multipass resonant PA cells or open PA cells. Most studies are performed with acoustically resonant cells equipped with a miniature electret microphone and cw radiation modulated at the resonance frequency. Since the PA signal is directly proportional to the absorbed power, the PA technique is a zero-background technique resulting in high sensitivity on the order of 10^{-9} cm^{-1}Hz$^{-1/2}$. New developments include a quartz-enhanced configuration named QEPAS [28] and a version with an interferometric detection of cantilever movement instead of a microphone [29].

Recently, cavity ring-down spectroscopy (CRDS) has successfully been employed in trace gas sensing [30, 31]. Modifications of the original approach include the use of cw radiation instead of pulsed radiation injected into the external cavity, then often called cavity leak-out spectroscopy (CALOS) [32] or an arrangement known as off-axis integrated cavity output spectroscopy (ICOS) [33]. These techniques are based on an external cavity with highly reflecting mirrors with a reflectivity of $\geq$ 99.99%. Instead of an absorption, a ring-down time is measured which has the advantage that laser power fluctuations do not influence the measurement. The calibration is easily done by comparing the ring-down time of the empty cavity with that of the cavity filled with the sample, i.e., no calibration gas is necessary as, e.g., in PAS. Owing to the long path length of kilometers realized with the external cavity, high sensitivities of typically 10^{-9} cm^{-1}Hz$^{-1/2}$ can be achieved. The drawback of the technique is the requirement for high-reflectivity mirrors which limits the usable wavelength range to some 10% of a central wavelength which is in contrast to PAS or multipass absorption spectroscopy where the same cell and mirrors can be used for different wavelength ranges. Furthermore, the laser beam quality is more critical than with the other techniques.

The selection of the detection scheme mainly depends on the laser source employed (particularly its wavelength range, power and beam quality), and the application requirements (particularly sensitivity and robustness).

4 Laser monitoring systems

In the following, the performance and potential of laser-based trace gas sensing systems is illustrated with examples of applications in diverse areas recently developed in our laboratory.

4.1 *Traffic emission measurements*

Within the frame of a measurement campaign, we demonstrated field sensing with an unattended mobile $^{12}CO_2$ – and $^{13}CO_2$ – laser-photoacoustic system employed for time-resolved street traffic emissions of ethylene (ethene, C_2H_4), ammonia (NH_3) and CO_2 [34]. The ambient air was pumped continuously through a resonant multipass PA cell equipped with 16 miniature microphones at a flow rate of 1.5 l/min. A typical PA spectrum (normalized with the incident laser power) is plotted in Fig. 1. It depicts the PA signals at both the $^{12}CO_2$ and $^{13}CO_2$ discrete laser transitions. Dominant lines of ammonia, ethene, CO_2 and water vapor absorption are indicated. During the measurement campaign, PA signals were recorded alternatively on appropriately selected CO_2 laser lines corresponding to prominent absorption lines of the gases of interest. Special attention was also given to the data analysis taking into account the so-called kinetic cooling effect [35, 36]. Figure 2 shows simultaneous recordings of three compounds during one week. The traffic counts per 10 minutes for light and heavy vehicles are also indicated. A good correlation between the derived concentrations of the gas compounds and the traffic count was observed, however, somewhat less pronounced for ammonia. Morning and evening peaks with concentrations of > 2000 ppm for CO_2, up to 400 ppb for C_2H_4 and > 600 ppb for NH_3 were clearly visible during weekdays and rather broad distributions over the weekend. The NH_3 peaks appeared slightly broader, and usually slightly delayed with

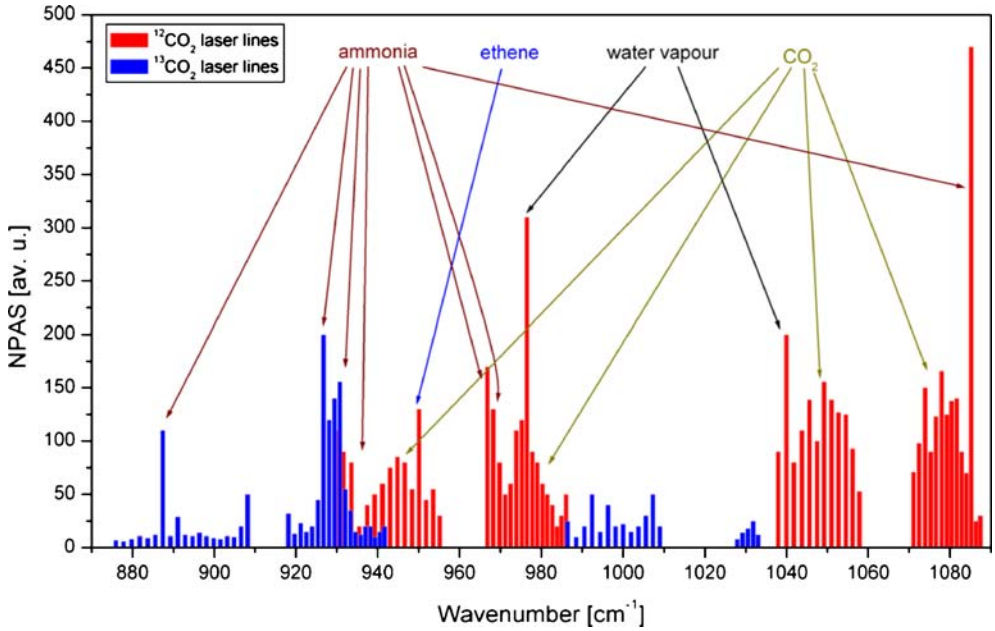

FIGURE 1 Photoacoustic spectrum of air sampled at exit of street tunnel. The photoacoustic signal amplitude (normalized by laser power) is plotted for the $^{12}CO_2$ and $^{13}CO_2$ laser transitions. The data are taken at atmospheric pressure and ambient temperature. Dominant gas lines of ammonia, ethene, water vapor and CO_2 are indicated by *arrows*

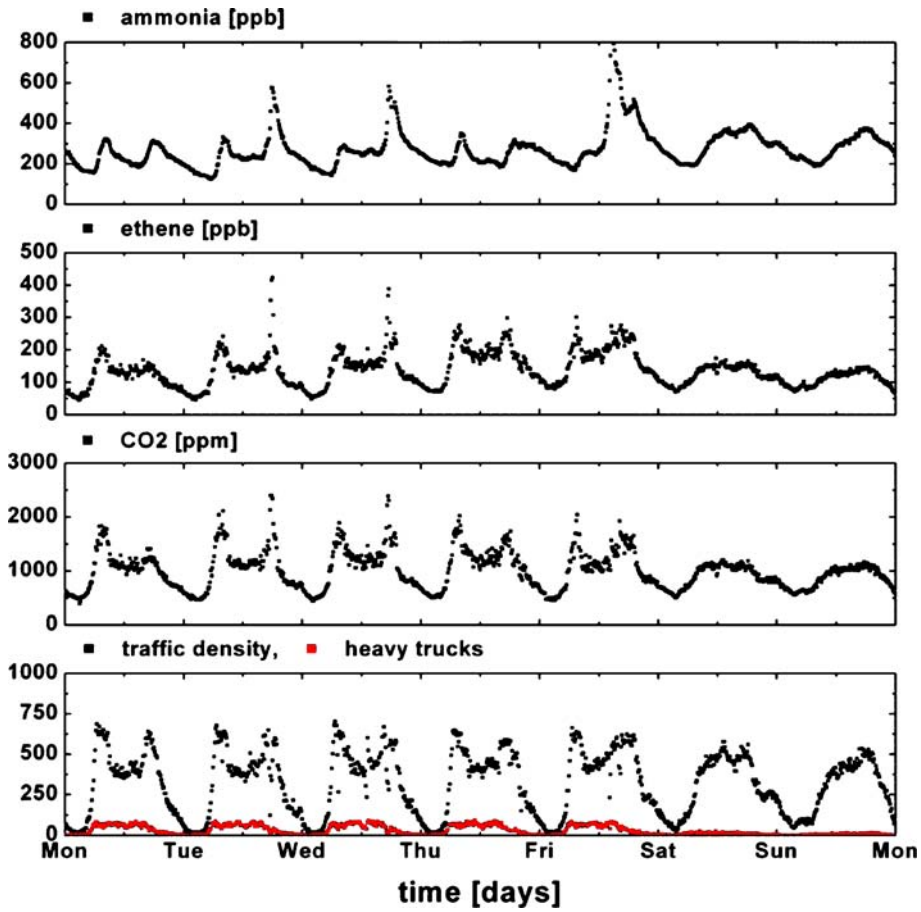

FIGURE 2 Temporal development of derived ammonia, ethene and CO_2 concentrations as well as traffic counts during one week at a street tunnel exit near Zurich, Switzerland. The traffic counts indicate the total number of all vehicles per 10 min as well as the number of heavy vehicles with lengths > 5.5 m (bottom curve with almost no trucks on weekends)

respect to the peak concentrations of the other gases presumably caused by adsorption/desorption processes in the teflon inlet tube and at the cell walls. This was also manifested in the temporal fluctuations of concentrations (related to the fluctuating traffic count), which were again less pronounced for NH_3. The measured gas concentrations were all well above the detection limits of the system, amounting to 70 ppt for both C_2H_4 and NH_3 under interference-free conditions.

The temporal evolution and/or typical gas average concentrations were all confirmed in this campaign by independent measurements with other instrumentation like FTIR, differential optical absorption spectroscopy (DOAS, UV range), gas chromatography, impinger, denuder, etc. [37]. In combi-

nation with the traffic flow data, emission factors could be determined: for NH_3, a factor of 31 ± 4 mg/km for light-duty vehicles (essentially cars) and 14 ± 7 mg/km for heavy-duty vehicles (mainly trucks) could be derived. Our measurements demonstrate that in situ laser-based PA measurements with a fully automated stand-alone system are feasible for time-resolved recording of selected compounds even in an extremely noisy and dusty environment with a vibrating ground and ever changing conditions.

4.2 *Near-IR industrial gas sensing*

In collaboration with an industrial partner, we performed a feasibility study for on-line sensing of acetylene (C_2H_2) contaminants at the sub-ppm level in an ethylene (ethene, C_2H_4) carrier gas flow [38]. This has important implications for the petrochemical industry as impurities such as C_2H_2 play a crucial role for the production of plastics which demand pure C_2H_4. Currently, such measurements are performed by GC. This well-established technique is, however, operating at its limit of detection and the preferred temporal resolution for true on-line measurements is not met by GC. We used a fiber-coupled cw ECDL tunable around 1530 nm and a homemade cavity ringdown cell equipped with two mirrors of $> 99.99\%$ reflectivity and a piezo-electric modulator for sweeping the cavity length to ensure the excitation of a single fundamental longitudinal cavity mode. An acousto-optic modulator was inserted into the laser beam before entering the fiber to switch off the laser beam immediately after the incident laser frequency had matched a cavity mode frequency. The radiation leaking out of the cavity was recorded with a fast InGaAs photodiode. With this rather simple, robust and economical set-up for industrial applications, and a laser power of only 1.4 mW and a PZT sweeping rate of only 10 Hz, we achieved a minimum detectable absorption coefficient $\alpha_{\min} = 4.5 \times 10^{-8}\,\mathrm{cm^{-1}Hz^{-1/2}}$ for a signal-to-noise ratio SNR = 1. After careful selection of the most appropriate wavelength by tuning the ECDL, the C_2H_2 P(9) line at 1530.3718 nm [39] was found to suffer least from absorption interference with the C_2H_4 background. Above sensitivity corresponds to a C_2H_2 detection limit of 20 ppb at 100 mbar total pressure under interference-free conditions which increases to 160 ppb in the background of C_2H_4. This limit was demonstrated with a linear plot of derived absorption coefficient versus C_2H_2 concentration added to the normal C_2H_4 flow at a time resolution of 1 min. The results are depicted in Fig. 3. At a flow rate of 200 $\mathrm{cm^3/min}$ and 20 mbar cell pressure, C_2H_2 was added stepwise to the C_2H_4 flow while the cell was flushed with pure C_2H_4 after 80 minutes.

4.3 *Isotope-ratio measurements*

In addition to general trace gas sensing, the isotopic compositions of certain species are often of great interest as they enable conclusions on the origins of the species as well as their uses as tracers. Application fields include ecological gas exchange, volcanic emission, medical diagnostics, extraterrestrial atmospheres, etc. In ecosystem research, isotope ratios of molecules such as CO_2, H_2O, N_2O, NO and NO_2 [40] are of interest as they may enable the identification of their origin. As example, CO_2 may originate from natural sources (soil and plants) but also from anthropogenic activity (combustion, etc.), yet the isotopic compositions are different for the different sources. In volcanic research, changes of isotope ratios of emitted volcanic gases can serve as indicators of increased volcanic activity and eventually be used for eruption forecast [41] in combination with seismic activity. A prominent example of medical diagnosis is the presence of Helicobacter pylori, the bacteria associated with peptic ulcers and gastric cancer, being manifested by increased $^{13}C/^{12}C$ isotope ratios recorded in exhaled CO_2 after intake of ^{13}C as a tracer into the body [42]. A further application concerns isotope ratio measurements in extraterrestrial atmospheres. As example, a near-IR tunable-diode-laser based instrument is being developed for future in-situ measurements of H_2O and CO_2 isotopes in the Martian atmosphere [43]. The isotope

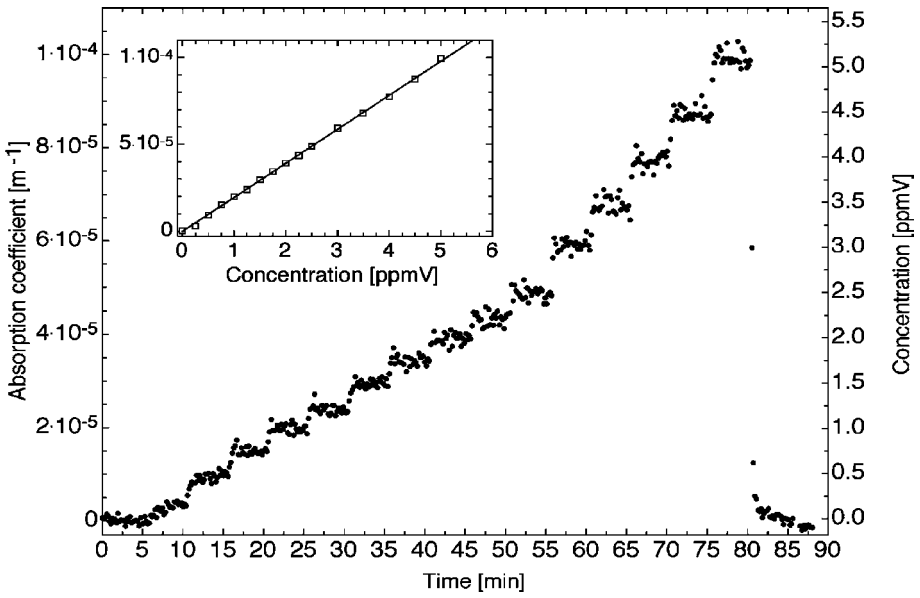

FIGURE 3 Gas-flow measurement of stepwise increasing acetylene (C_2H_2) concentrations in a flow of ethene (C_2H_4). The flow rate is 200 $\mathrm{cm^3/min}$ at a gas pressure of 20 mbar. The C_2H_2 concentration is increased stepwise in steps of 250 ppb until an added concentration of 2.5 ppm. After 55 min the concentration step is increased to 500 ppb. After 80 min the cell is flushed with pure C_2H_4

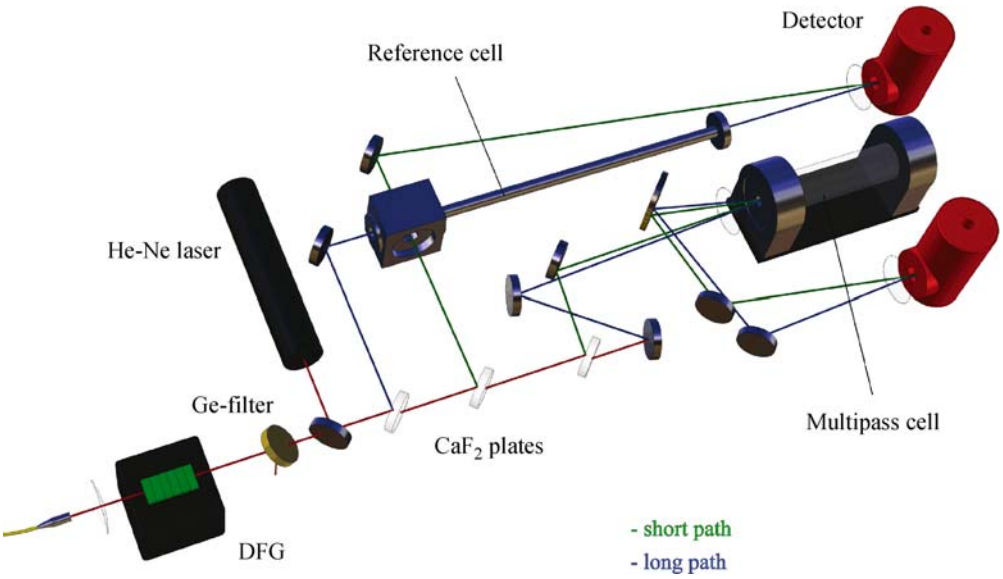

FIGURE 4 Experimental setup for balanced path length detection. The beam of the difference frequency generation (DFG) source is split into four beams with short and long paths through the multipass sample cell, as well as short and long paths through the reference cell. The He-Ne laser is used for beam alignment

ratio of a sample is normally compared to the one of a standard reference substance and the deviation of these ratios defines the so-called δ-value [44]:

$$\delta = \left(\frac{{}^{\text{minor}}\text{C}_{\text{sample}} / {}^{\text{main}}\text{C}_{\text{sample}}}{{}^{\text{minor}}\text{C}_{\text{ref}} / {}^{\text{main}}\text{C}_{\text{ref}}} - 1 \right) \times 1000‰ , \quad (1)$$

where ${}^{\text{main}}\text{C}$ denotes the concentration of the main isotope and ${}^{\text{minor}}\text{C}$ the one of the less abundant isotope, whereas the indices sample and ref correspond to sample gas and standard reference gas, respectively.

The standard method to determine isotope ratios is isotope-ratio-mass-spectrometry (IRMS), characterized by its excellent precision and accuracy on the order of 0.1‰ [45]. However, this instrument requires careful and time-consuming sample preparation and is rather bulky for field measurements. A promising alternative is laser spectroscopy which features an even better selectivity, good time resolution, no need for sample preparation and potential for field-deployable instrumentation. However, to achieve a similar performance at trace gas levels with laser spectroscopy, as with IRMS, presents a challenging task.

We implemented a mid-IR laser-spectroscopic system for simultaneous CO, CO_2 and N_2O isotope ratio measurements at trace concentrations. For a laser source, a cw DFG system was built consisting of a diode-pumped cw Nd:YAG laser (2W, Mephisto; InnoLight GmbH) as a signal laser at the fixed wavelength of 1064.5 nm, an ECDL (cw 150 mW, tunable 820–875 nm, Lynx; Sacher Lasertechnik) as pump laser and a 5 cm long MgO-doped periodically poled $LiNbO_3$ (MgO:PPLN) crystal inserted into a temperature-controlled oven (HC-Photonics) as a nonlinear optical mixing medium. For the idler wavelength range between 4.3 and 4.7 μm, we only used the PPLN grating with a periodicity of 23.1 μm, the ECDL tuning range of 852–868 nm and a temperature tuning of the oven between 30 °C and 130 °C. The idler power amounts to 23 μW at 4.3 μm and drops to 5 μW at 4.76 μm owing to increasing crystal absorption toward 5 μm. The linewidth amounts to approximately 1 MHz dominated by the ECDL linewidth of 1 MHz (the Nd:YAG laser linewidth is only 100 kHz). Recently, we also implemented a fiber-coupled DFG source which features a better idler beam shape, improved robustness and compactness, yet lower power owing to fiber coupling losses. This fiber-DFG system and its performance will be published elsewhere.

We combined our room-temperature DFG source with different detection schemes: direct absorption measurement with data acquisition card or wavelength modulation with first harmonic detection, only long path (10 m or 36 m) in sample cell, or balanced path length to take the different abundances and hence absorbances of isotopes into account. The experimental arrangement for balanced path length detection is depicted in Fig. 4. It shows four different path lengths, two of them through the sample cell (short path with just 1 mirror reflection, long path with 182 reflections for 36 m in total), and two of them through the reference cell with one path along and one path across the cell. We evaluated the performance of the systems with respect to reproducibility and time resolution. Table 3 lists the main results obtained for N_2O and CO isotope ratio measurements. In the case of N_2O, ratios of $^{14}N^{15}N^{16}O$ or of $^{15}N^{14}N^{16}O$ are of concern with respect to the main isotope $^{14}N_2^{16}O$; in the case of CO, it concerns the ratios of either $^{13}C^{16}O$ or $^{12}C^{18}O$ with respect to the main isotope $^{12}C^{16}O$.

It is obvious that the reproducibility improved substantially when using a dual-cell – (with sample and reference cell) instead of a single-cell – (only sample cell) set-up. The only long-path system was rather sensitive to temperature changes whereas the balanced path-length detection was much less prone to temperature changes but exhibited a worse S/N ratio because the power needed to be split into four beams instead of two. Similar performance is achieved for the free-space DFG and the fiber-coupled DFG system both combined with dual-cell arrangement with balanced path length and WM, yet the day-to-day reproducibility of the latter is much better. In fact, this improved day-to-day reproducibility now allows us to correct the δ-value for an often observed offset. Generally, the direct absorption scheme with data ac-

Method	Concentration	Reproducibility	Day-to-day reproducibility	Measurement time
Single cell, direct	2040 ppm N_2O	220‰	200‰	20 min
Dual-cell, only long path, WM	825 ppm N_2O	6‰*	30‰	20 min
Balanced pathlengths, WM	825 ppm N_2O	10‰	40‰	20 min
Dual cell, only long path, direct	825 ppm N_2O	15‰	28‰	15 s to 6 min
Balanced pathlengths, direct	825 ppm N_2O	6‰	–	15 s to 6 min
Fiber-coupled, WM	100 ppm N_2O	9‰	6‰	12 min
Single cell, balanced pathlengths, direct	200 ppm CO	150‰	160‰	20 min
Dual-cell, balanced pathlengths, WM	300 ppm CO	11‰	30‰	20 min
Dual-cell, balanced pathlengths, direct	300 ppm CO	4.7‰	15‰	15 s to 6 min

*including temperature changes, this value increases to 18‰

TABLE 3 Comparison of different measurement methods used (WM: wavelength modulation, direct: direct absorption spectroscopy, reproducibility: with respect to measurements performed the same day), system: free-space DFG unless otherwise indicated

quisition card yields the best time resolution. It should also be mentioned that isotope ratios like $^{14}N^{15}NO/^{15}N^{14}NO$ can be determined in a straightforward manner in contrast to IRMS, which does not enable a direct determination due to identical masses of these two isotopes. It is the first time that N_2O isotope ratios have been measured with laser spectroscopic methods at these trace levels [46]. A more detailed report on the CO measurements will be published elsewhere. Although the achieved precision – usually in the range of a few ‰ – as well as the reproducibility are not yet sufficient for actual field measurements where ambient concentrations amount to typically 320 ppb and precisions $\Delta\delta$ and reproducibilities of < 1‰ are required, further developments with higher laser power and temperature-controlled sample and reference cells are expected to considerably increase the future system performance.

4.4 *Breath analysis*

Exhaled human breath is a complex gas mixture containing hundreds of different species [47–50]. The most prominent ones are nitrogen, oxygen, carbon dioxide and water vapor, yet there are traces of numerous other gases and volatile organic compounds (VOCs) present. Recent studies in medicine and clinical toxicology – mainly performed by gas chromatography combined with mass spectrometry (GC-MS) – suggest certain correlations between the presence and concentration of specific trace gases (e.g., nitric oxide, carbon monoxide, ethane, isoprene, acetone, amines, and sulphides) and several common disorders like liver disease, lung cancer, heart disease, exposure to environmental toxins, schizophrenia, uncontrolled diabetes and malnutrition [51]. It has been recognized rather early that such correlations could be used to establish a new noninvasive diagnostic tool based on the quantification of certain compounds or mixtures of compounds in exhaled air. The correlation between exhaled compounds and specific diseases, however, is often ambiguous and it would therefore be helpful to sense several trace gases in the breath simultaneously to increase both the specificity and the reliability of diagnosis.

The main challenges are related to the low concentrations ($\leq$ ppb) of many compounds in breath and the strong interference by the dominant gases. In the IR range this concerns CO_2 and H_2O vapor which are both present in the percent range. With the relevant features of high sensitivity and specificity, IR laser spectroscopy holds a great potential for medical diagnostics [52–54].

In a recent project we focused on the detection of methylamines in human breath as possible tracers for liver or renal diseases [55, 56]. The first spectroscopic studies were performed on air samples containing given concentrations of monomethylamine (MMA, $(CH_3)NH_2$); dimethylamine (DMA, $(CH_3)_2NH$) and trimethylamine (TMA, $(CH_3)_3N$). The chemical structures of these compounds are depicted in Fig. 5. As these methylamines are polar molecules, they have a strong affinity to stick to surfaces. In order to prevent fluctuations of their concentrations, we designed and used a constant flow generation and handling system comprising a fixed flow of nitrogen as buffer gas through a permeation chamber where a sample of liquid methylamine solution was kept in a sealed teflon tube at constant temperature and gas flow rate. The chamber temperature and the N_2 flow rate enable a control of the methylamines between 1 and 1000 ppm [57].

In the near-IR range we used an ECDL combined with cavity ringdown spectroscopy (CRDS), whereas a DFG multipass absorption spectrometer was employed in the mid-IR. The first overtone of the NH stretch vibration at 1505–1550 nm was probed and a minimum detectable absorption coefficient $\alpha_{\min} = 1.55 \times 10^{-8}\,\mathrm{cm}^{-1}$ (for SNR = 1) was achieved. This corresponds to 350 ppb for MMA and 1.6 ppm for DMA under interference-free conditions in synthetic gas mixtures. If the interferences with H_2O and CO_2 in exhaled air are taken into account these limits increase to 10 and 60 ppm for MMA and DMA, respectively, for SNR = 1. These latter concentrations are still 3–4 orders of magnitude too high to ensure a medical diagnosis. Furthermore, TMA cannot be sensed in the near-IR as there is no N−H stretch vibration and hence also no overtone (see Fig. 5).

In the mid-IR region, the fundamental C−H stretch vibrations of all three methylamines can be sensed. As in the isotope-ratio measurements (see Sect. 4.3), we implemented

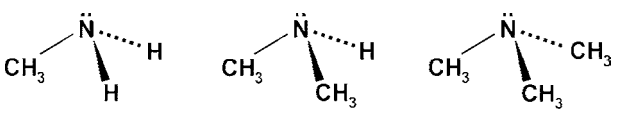

FIGURE 5 Chemical structures of methylamines (from *left* to *right*); MMA: monomethylamine (CH_3NH_2), DMA: dimethylamine $(CH_3)_2NH$, TMA: trimethylamine $(CH_3)_3N$. Note that TMA does not exhibit a N−H bond

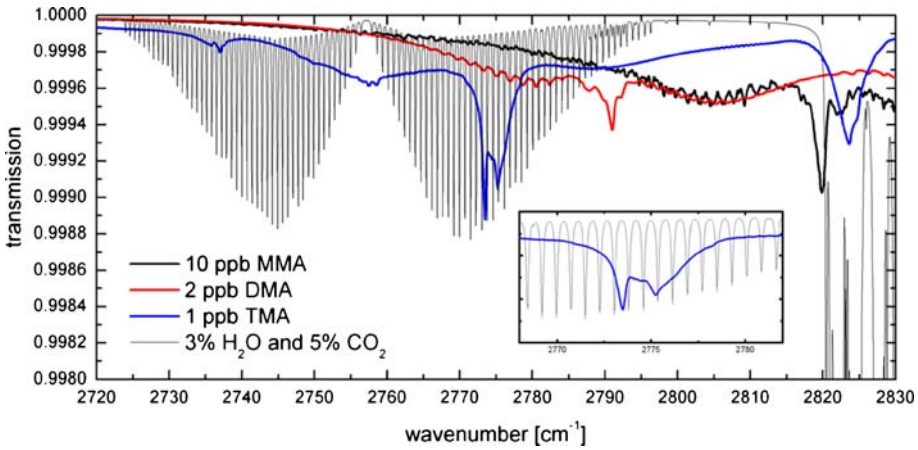

FIGURE 6 Calculated spectra of methylamines (MMA, DMA and TMA) according to the PNNL database [58] at ppb concentrations, in presence of 3% H_2O and 5% CO_2 [59]. In contrast to the near-IR region, no interferences are occurring as the *inset* indicates

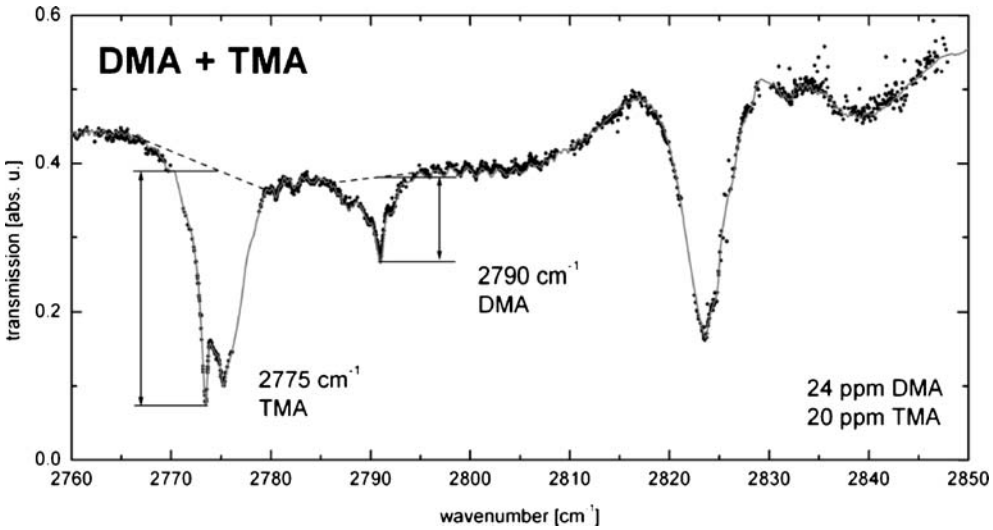

FIGURE 7 Wide scan of a mixture of 24 ppm DMA and 20 ppm TMA diluted in a nitrogen flow at 950 mbar total pressure with the cw-DFG system. The gaps in the transmission spectrum are caused by the random nature of step-motor tuning of the ECDL signal laser. The *solid line* represents the corresponding transmission according to the PNNL database [58]

a mid-IR source based on DFG between a diode-pumped Nd:YAG laser and an ECDL in the 815–835 nm range yielding cw idler radiation between 3.5 and 3.9 μm. As the power is in the μW range, we used again long-path absorption and ratiometric detection yielding a minimum detectable absorption coefficient $\alpha_{\min} = 3.8 \times 10^{-6}\,\mathrm{cm}^{-1}$ for SNR = 1. With an averaging time of 300 ms of the lock-in amplifiers, this corresponds to a sensitivity of $2 \times 10^{-6}\,\mathrm{cm}^{-1}\mathrm{Hz}^{-1/2}$. This limit is apparently 2 orders of magnitude worse than what we achieved with higher laser power and CRDS detection in the near-IR. However, since the absorption cross sections in the mid-IR are higher, the minimum detectable concentrations become similar. Even more important is the fact that all three methylamines can be measured without interference from H_2O vapor and/or CO_2 present at the percent level. The situation is presented in Fig. 6 with calculated spectra for MMA, DMA and TMA according to the PNNL database [58] at ppb concentrations in the presence of 3% H_2O vapor and 5% CO_2 (Hitran database [59]), as typically encountered in human breath.

Since all methylamines feature C−H bonds and since at least one methyl group is present in all of them, it is a challenging task to distinguish between them. Figure 7 presents a measurement of a mixture consisting of (24 ± 1.2) ppm DMA and (20 ± 1.2) ppm TMA at 950 mbar total pressure.

species	line position [cm^{-1}]	max. absorption cross section [cm^2]	detection limit (SNR = 1)
MMA	2823	1.8×10^{-19}	900 ppb
DMA	2790	3.7×10^{-19}	450 ppb
TMA	2775	1.3×10^{-18}	120 ppb

TABLE 4 Absorption features and detection limits of the methylamines in the mid-IR

A clear distinction is easily achieved with two absorption peaks at 2775 cm^{-1} and 2823 cm^{-1} for TMA and one intermediate absorption peak at 2790 cm^{-1} owing to DMA absorption. Since the characteristic narrow absorption lines of each gas are positioned in regions of flat background absorption of the other gas in the mixture, only intermediate accuracies could be realized. Table 4 lists the absorption data derived. The detection limits (SNR = 1) given apply for interference-free conditions but are identical for breath samples with the usual CO_2 and H_2O vapor concentrations as interference does not occur in the chosen mid-IR range.

4.5 *Analysis of vapors*

From time to time, doping affairs in sports appear in the headlines. The doping controls are conducted in 36

accredited laboratories worldwide. The challenging analyses require highly sensitive and selective instrumentation and at the same time the results should be available quickly. The illegal doping agents taken by athletes are currently detected in urine samples primarily using gas and liquid chromatography coupled to mass spectrometry (GC-MS and LC-MS) [60]. Although these well established techniques yield excellent sensitivity limits, the sample preparations are sophisticated and time consuming. Complementary methods would thus be welcome, also methods that enable clear and easy structural differentiation. An example is ephedrine which is prohibited for its stimulatory effects when its concentration in urine exceeds 10 μg/ml, whereas pseudoephedrine, its rather inactive diastereoisomer, is legal.

First, spectroscopic studies with a broadband (8 cm^{-1}) optical parametric generator were aimed at recording vapor-phase spectra of various doping agents of different classes (anabolics, stimulants, beta blockers and diuretics) [61]. In the current project, we employ a narrowband DFG source based on a pulsed diode-pumped Nd:YAG laser (pulse duration: 6 ns, peak power: 5 kW, pulse repetition rate: 4–8 kHz; InnoLight) as a pump laser, a cw ECDL (tuning range: 1520–1600 nm, power: 5–9 mW, linewidth: < 4 MHz; Santec or EOSI/Newport) as a signal laser and PPLN as a nonlinear mixing medium. This laser source is equipped with an automated wavelength control. The idler radiation can be tuned either across a wide range of 329 cm^{-1} (between 2815 cm^{-1} and 3144 cm^{-1} , i.e., between 3.18 μm and 3.55 μm) with a step-width of 0.04 to 0.4 cm^{-1} with a fully computer-controlled step motor and PPLN temperature control, or within a narrow range of 1–2 cm^{-1} with a piezoelement. The average power is < 1 mW with a linewidth of 150 MHz. The extraordinarily broad tuning range is crucial for spectroscopically analyzing doping agents as well as other large molecules as they exhibit broad absorption features in the mid-IR region.

In order to study molecules in the vapor phase at elevated temperatures, we developed a high-temperature multipass cell [62] of Herriott type which is heatable up to 600-700 K depending on the window sealing type, with an accuracy of ±1 K. The total optical path length can be varied between 9 and 35 m. The cell mirrors are heated separately to slighty above the cell temperature in order to avoid condensation. After initial test measurements on water vapor and methane at elevated temperatures, we continued with measurements on acetone vapor. Acetone ($(CH_3)_2CO$) exhibits 24 vibrational modes, grouped into 8 of symmetry species A_1, 4 of A_2, 7 of B_1 and 5 of B_2 [63]. Acetone is not only of spectroscopic interest because it plays an important role in tropospheric chemistry [64, 65] and is found in interstellar space [66–68], but also because it is present at elevated concentrations in exhaled breath of patients with diabetes or patients on ketogenic diets [69–71] and therefore is referred to as a biomarker for diabetes. Although no laser-based detection of acetone in real breath samples has been reported so far, there is great interest in such devices. Recently, acetone has been measured in a mixture with Freon 125 with an EC-QCL with a wide tuning range of 135 cm^{-1} around 8.4 μm combined with QEPAS [72]. The retrieved acetone spectrum enabled the determination of a detection limit for acetone in the ppb range. In earlier measurements we used a CO laser PA spectrometer and derived a limit of 4.2 ppb for acetone in the region of the strong carbonyl stretching vibration around 1740 cm^{-1} [73]. In Fig. 8 we present two spectra of acetone vapor in the (weaker) C−H stretching absorption region around 3000 cm^{-1} measured in our high-temperature multipass cell with a total path length of 31.7 m at 296 K and 400 K. The measured spectra represent single scans taken on 1665 ppm acetone buffered in 100 mbar of N_2 at 296 K and 130 mbar N_2 at 400 K. The room-temperature spectrum is compared with an FTIR spectrum recorded at 1 atm with a spectral resolution of 0.125 cm^{-1}. Despite the different total pressures, excellent agreement is observed because the rotational lines overlap even under our reduced pressure conditions, resulting in a continuous contour of the absorption spectrum. The FTIR spectrum was only scaled in the absorbance axis to fit our experimental conditions.

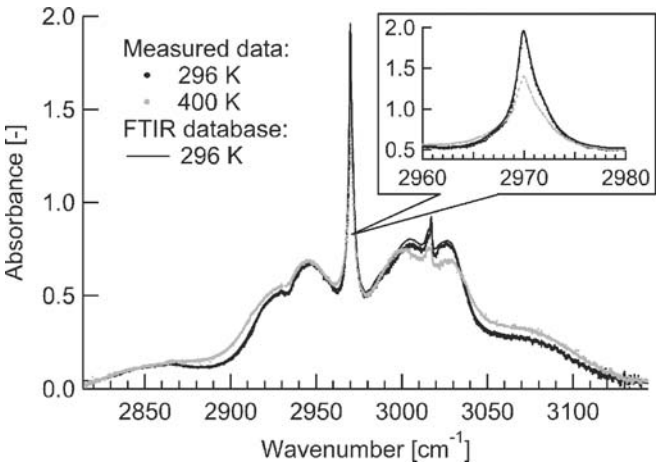

FIGURE 8 C−H stretching absorption band of acetone. A room-temperature FTIR spectrum is compared to single scans of 1665 ppm acetone buffered in 100 mbar N_2 at 296 K and in 130 mbar N_2 at 400 K, respectively. The *inset* shows the enlarged main peak at 2970 cm^{-1} at the two temperatures

Assignment	Wavelength ν [cm^{-1}]		Abs. cross section [10^{-21} cm^2]	
	calculated	measured	$T = 296$ K	$T = 400$ K
$\nu_2(A1)$, $\nu_{14}(B1)$	2926	2929.4 ± 0.1	41 ± 4	
$\nu_9(A2)$, $\nu_{20}(B2)$	2973	2970.0 ± 0.1	152 ± 15	108 ± 11
$\nu_1(A1)$, $\nu_{13}(B1)$	3020	3017.2 ± 0.1	70 ± 7	

TABLE 5 C−H stretching vibrational modes, assignments and effective cross sections of acetone at temperatures of 296 K and 400 K

The three distinctive features could be assigned to C−H stretching vibrational modes taken from theoretical work [74]. The assignments and measured effective absorption cross sections are listed in Table 5.

The weak mode at 2929.4 cm^{-1} is hardly visible in Fig. 8 but can clearly be distinguished in the data. Another weak peak which appears at 2942.0 ± 0.1 cm^{-1} and the broad band, centered around 2947 cm^{-1}, could not be assigned. The error in the observed wavenumber is given by the chosen step width of 0.08 cm^{-1} to record the spectrum. The indicated errors in the effective absorption cross section is dominated by the uncertainty of the injected volume of acetone into the cell. Taking the effective cross section at 2970 cm^{-1} and a noise level of 0.3% (transmission scale) as derived from indepen-

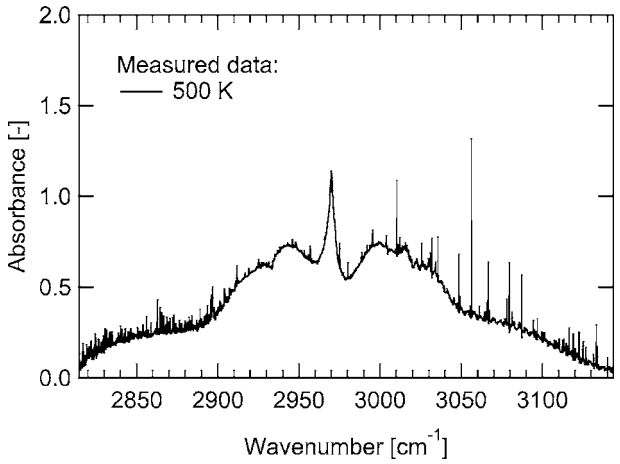

FIGURE 9 Signs of degradation at 500 K in the C−H stretching vibration band of acetone. The spectrum was recorded with 1665 ppm acetone buffered in 170 mbar N_2. The *narrow lines* above 3000 cm^{-1}, e.g. at 3010.231 or 3056.357 cm^{-1} can be assigned to water vapor, whereas the numerous lines below 3000 cm^{-1} are predominantly caused by formaldehyde (CH_2O) absorption

dent measurements on gases, a detection limit of 760 ppb acetone in 1 atm N_2 can be projected for SNR = 3. In addition, we recorded a spectrum at 400 K which deviates from the one taken at 296 K. In particular, the main peak at 2970 cm^{-1} decreases as a result of lower state depopulation as clearly visible in the inset of Fig. 8. In contrast to a common FTIR spectrometer, we could easily increase the temperature of our cell further. An acetone spectrum taken at 500 K is depicted in Fig. 9.

First signs of degradation of acetone are visible at this temperature. In addition to the broad acetone absorption, narrow lines appear in the spectrum that are resolved due to the narrow laser linewidth. Whereas the lines above 3000 cm^{-1}, e.g. at 3010.231 cm^{-1} or 3056.357 cm^{-1}, could be identified as water vapor, the numerous lines below 3000 cm^{-1}, e.g. at 2824.658 cm^{-1} or 2830.652 cm^{-1}, are predominantly caused by absorption of formaldehyde (CH_2O). These lines presumably originate from acetone oxidation caused by an increase of O_2 concentration in the cell [75]. Although the reproducibility of this measurement was not further investigated, it indicates the magnitude of the consequences of a possible leak at higher temperatures.

Most recently, we performed the first analyses of prepared urine samples in the vapor phase in our cell. The first results clearly indicate the unambiguous differentiation between blank urine, urine with added ephedrine at concentrations close to the level prohibited in sports and urine with added pseudoephedrine. The results of these studies will be published elsewhere [76].

5 Conclusion and outlook

Laser-based detection devices for trace gas sensing fulfill most requirements with respect to multi-component capability, sensitivity, specificity, time resolution, field deployment, etc. The ideal system combination in terms of laser source and detection method strongly depends on the application. Several systems and their performance in various applications have been discussed. An automated CO_2-laser photoacoustic system has demonstrated its suitability for street traffic emission sensing in a harsh environment. Concentrations of CO_2, ethene and ammonia have been continuously recorded during several weeks with a time resolution of 5 min. In an industrial collaboration, a near-IR system with an external cavity diode laser and a cavity ringdown cell has been implemented and applied to the laboratory measurements of acetylene traces in a background flow of technical grade ethene. Added acetylene concentrations of 160 ppb could be recorded with a time resolution of 1 min. Instead of a conventional gas-chromatography mass spectrometry (GC-MS) system, with inferior temporal resolution, such a laser-based device could be of interest for direct implementation into a polyethylene production site.

Isotope ratio measurement is another area where laser spectroscopy is of great interest, owing to the high spectral resolution which also enables site-selective isotope differentiation, e.g., between $^{14}N^{15}N^{16}O$ and $^{15}N^{14}N^{16}O$ where conventional mass spectrometry cannot provide direct measurements. We present a free-space and a fiber-coupled DFG system for isotope ratio measurements of N_2O, CO and CO_2 at ppm concentrations, all with a single device. Direct absorption and wavelength modulation as well as different types of cell configurations including balanced path lengths with sample and reference cell have been compared. Although the desired precision and reproducibility of $< 1‰$ has not been achieved yet in this study, current developments in terms of laser devices with higher power and better spectral purity, such as widely tunable QCLs as well as the use of temperature-controlled sample and reference cells, will yield the desired precision combined with better time resolution and field capability, and hence be competitive with the isotope ratio mass spectrometry (IRMS) technique.

Noninvasive medical diagnosis using breath analysis is another topic of great interest. We have discussed the detection of methylamines considered as biomarkers for liver and renal diseases. Both a near-IR cavity ring-down and a mid-IR DFG-based multipass absorption system have been implemented. Detectable concentrations in the carefully selected interference-free wavelength range between 2740–2860 cm^{-1} are 900 ppb for mono-methylamine, 450 ppb for di-methylamine and 120 ppb for tri-methylamine, even with 3% H_2O and 5% CO_2 usually present in human breath. These values are still 2 orders of magnitude above actual methylamines concentrations in breath. However, with higher laser powers becoming available in above wavelength range (either with waveguide DFG sources or eventually QCLs), the laser source could be combined with a cavity ring-down cell yielding the desired high sensitivity.

Finally, a new type of high-temperature multipass Herriott cell and an extremely broadly tunable DFG source (tuning range > 300 cm^{-1}) are presented. This system is being used for absorption studies on condensable vapors and large molecules. For example, the whole C−H stretching band of acetone vapor has been measured between 2810 and 3140 cm^{-1} at temperatures of 296 K, 400 K and 500 K. The room temperature spectrum agrees very well with a FTIR spectra. At 500 K, however, first signs of acetone degra-

dation were found and could be assigned to water vapor and formaldehyde formation. In a current project, we employed this system to detect doping agents in urine. Ephedrine (used as stimulant in sports) and its diastereoisomer pseudoephedrine could be clearly distinguished. This example demonstrates another successful application and opens the pathway to new areas in which laser sensors could play an important role in the future.

ACKNOWLEDGEMENTS We thank Romedi Selm for practical assistance regarding the isotope measurements. The financial support for the different projects discussed in this work by the Swiss National Science Foundation, ETH Zurich, ABB Research Laboratory and the GEBERT RÜF STIFTUNG is gratefully acknowledged.

REFERENCES

1 F.K. Tittel, A.A. Kosterev (guest eds.), Appl. Phys. B **85**, No. 2-3 (2006)
2 A. Romann, M.W. Sigrist, Appl. Phys. B **75**, 377 (2002)
3 P. Repond, M.W. Sigrist, IEEE J. Quantum Electron. **QE-32**, 1549 (1996)
4 S. Li, Q. Yu, M. v. Herpen, S. t. L. Hekkert, F.J.M. Harren, Chin. Opt. Lett. **1**, 361 (2003)
5 I.T. Sorokina, E. Sorokin, A. Di Lieto, M. Tonelli, R.H. Page, K.I. Schaffers, J. Opt. Soc. Am. B **18**, 926 (2001)
6 J.J. Adams, C. Bibeau, R.H. Page, D.M. Krol, L.H. Furu, S.A. Payne, Opt. Lett. **24**, 1720 (1999)
7 R.Q. Yang, C.J. Hill, B.H. Yang, Appl. Phys. Lett. **87**, 151 109 (2005)
8 K. Mansour, Y. Qiu, C.J. Hill, A. Soiber, R.Q. Yang, Electron. Lett. **42**, 1034 (2006)
9 C.J. Hill, C.M. Wong, B. Yang, R.Q. Yang, Electron. Lett. **40**, 878 (2004)
10 M. Tacke, F. Wienhold, R. Grisar, H. Fischer, F.-J. Lübken, in: *Encyclopedia of Analytical Chemistry*, ed. by R.A. Meyers, Vol. 3, Section *Environment: Trace Gas Monitoring*, ed. by M.W. Sigrist (Wiley, Chichester, UK, 2000), pp. 2033–2065
11 P. Werle, F. Slemr, K. Maurer, R. Kormann, R. Mücke, B. Jänker, Opt. Lasers Eng. **37**, 101 (2002)
12 K. Kellermann, D. Zimin, K.M. Alchalabi, P. Gasser, N.A. Pikhtin, H. Zogg, J. Appl. Phys. **94**, 7053 (2003)
13 J. Fürst, H. Pascher, T. Schwarzl, M. Böberl, G. Springholz, G. Bauer, W. Heiss, Appl. Phys. Lett. **84**, 3268 (2004)
14 J. Faist, F. Capassso, D.L. Sivco, C. Sirtori, A.L. Hutchinson, A.Y. Cho, Science **264**, 553 (1994)
15 S.R. Darvish, S. Slivken, A. Evans, J.S. Yu, M. Razeghi, Appl. Phys. Lett. **88**, 201 114 (2006)
16 A. Wittmann, M. Giovannini, J. Faist, L. Hvozdara, S. Blaser, D. Hofstettter, E. Gini, Appl. Phys. Lett. **89**, 141 116 (2006)
17 R. Maulini, A. Yarekha, J.-M. Bulliard, M. Giovannini, J. Faist, E. Gini, Opt. Lett. **30**, 2584 (2005)
18 G. Wysocki, R.F. Curl, F.K. Tittel, R. Maulini, J.M. Bulliard, J. Faist, Appl. Phys. B **81**, 769 (2005)
19 M. Ebrahimzadeh, in: *Solid-State Mid-Infrared Laser Sources*, ed. by I.T. Sorokina, K.L. Vodopyanov, Top. Appl. Phys., Vol. 89 (Springer, Berlin Heidelberg, 2003), pp. 179–218
20 A.K.Y. Ngai, S.T. Persijn, G. von Basum, F. Harren, Appl. Phys. B **85**, 173 (2006)
21 C. Fischer, M.W. Sigrist, in: *Solid-State Mid-Infrared Laser Sources*, ed. by I.T. Sorokina, K.L. Vodopyanov, Top. Appl. Phys., Vol. 89 (Springer, Berlin Heidelberg, 2003), pp. 97–140
22 H. Wächter, M.W. Sigrist, in: *Laser Handbook*, ed. by F. Träger (Springer, Berlin Heidelberg, 2007), Chapt. 11.10, pp. 801–814
23 J.U. White, J. Opt. Soc. Am. **32**, 285 (1942)
24 D. Herriott, H. Kogelnik, R. Kompfner, Appl. Opt. **3**, 523 (1964)
25 A.G. Bell, Am. J. Sci. **20**, 305 (1880)
26 A. Miklos, P. Hess, Z. Bozoki, Rev. Sci. Instrum. **72**, 1937 (2001)
27 M.W. Sigrist, in: *Air Monitoring by Spectroscopic Techniques*, ed. by M.W. Sigrist, Chemical Analysis Series, Vol. 127 (Wiley, New York, 1994), pp. 163–238
28 A.A. Kosterev, F.K. Tittel, D.V. Serebryakov, A.L. Malinovsky, L.V. Morozoy, Rev. Sci. Instrum. **76**, 043 105 (2005)
29 T. Laurila, H. Cattaneo, V. Koskinen, J. Kauppinen, R. Hernberg, Opt. Express **13**, 2453 (2005)
30 K.W. Busch, M.A. Busch (eds.), *Cavity-Ringdown Spectroscopy – An Ultratrace-Absorption Measurement Technique*, ACS Symp. Ser., Vol. 720 (Amer. Chem. Soc., Washington, 1999)
31 G. Berden, R. Peeters, Int. Rev. Phys. Chem. **19**, 565 (2000)
32 D. Halmer, G. von Basum, M. Horstjann, P. Hering, M. Mürtz, Isotopes Environ. Health Stud. **41**, 303 (2005)
33 Y.A. Bakhirkin, A.A. Kosterev, R.F. Curl, F.K. Tittel, D.A. Yarekha, L. Hvozdara, M. Giovannini, J. Faist, Appl. Phys. B **82**, 149 (2006)
34 D. Marinov, M.W. Sigrist, Photochem. Photobiol. Sci. **2**, 774 (2003)
35 A.D. Wood, M. Carmac, E.T. Gerry, Appl. Opt. **10**, 1877 (1971)
36 R.A. Rooth, A.J.L. Verhage, L.W. Wouters, Appl. Opt. **29**, 3643 (1990)
37 L. Emmenegger, J. Mohn, M.W. Sigrist, D. Marinov, U. Steinemann, F. Zumsteg, M. Meier, Int. J. Environ. Poll. **22**, 326 (2004)
38 D.E. Vogler, M.W. Sigrist, Appl. Phys. B **85**, 349 (2006)
39 R. El Hachtouki, J. Vander Auwera, P. Varanasi, G. Wagner, J. Mol. Spectrosc. **216**, 355 (2002)
40 D. Yakir, L.S.L. Sternberg, Oecologia **123**, 297 (2000)
41 A. Castrillo, G. Casa, M. van Burgel, D. Tedesco, L. Gianfrani, Opt. Express **12**, 6515 (2004)
42 S. Koletzko, M. Haisch, I. Seeboth, B. Braden, K. Hengels, B. Koletzko, P. Hering, Lancet **345**, 91 (1995)
43 T. le Barbu, B. Parvitte, V. Zeninari, I. Vinogradov, O. Korablev, G. Durry, Appl. Phys. B **82**, 133 (2006)
44 H. Craig, Cosmochim. Geochim. Acta **12**, 133 (1957)
45 T. Röckmann, J. Kaiser, C.A.M. Brenninkmeijer, W.A. Brand, Rapid Commun. Mass Spectrom. **17**, 1897 (2003)
46 H. Wächter, M.W. Sigrist, Appl. Phys. B **87**, 539 (2007)
47 M. Phillips, Sci. Am. **267**, 74 (1992)
48 S.S. Sehnert, L. Jiang, J.F. Burdick, T.H. Risby, Biomarkers **7**, 174 (2002)
49 A. Amann, D. Smith (eds.), *Breath Analysis for Clinical Diagnosis and Therapeutic Monitoring* (World Scientific, Singapore, 2005)
50 T.H. Risby, S.F. Solga, Appl. Phys. B **85**, 421 (2006)
51 S.A. Kharitonov, P.J. Barnes, Am. J. Resp. Crit. Care Med. **163**, 1693 (2001)
52 G. von Basum, H. Dahnke, D. Halmer, P. Hering, M. Mürtz, J. Appl. Physiol. **95**, 2583 (2003)
53 A. Kosterev, F.K. Tittel, IEEE J. Quantum Electron. **QE-38**, 582 (2002)
54 K.L. Moskalenko, A.I. Nadzhdinskii, I.A. Adamovskaya, Infrared Phys. Technol. **37**, 181 (1996)
55 M.L. Simenhoff, J.F. Burke, J.J. Saukkonen, A.T. Ordinario, R. Doty, New Engl. J. Med. **297**, 132 (1977)
56 S. Mitchell, R. Ayesh, T. Barrett, R. Smith, Scand. J. Gastroenterol. **34**, 524 (1999)
57 D. Marinov, J.M. Rey, M.G. Müller, M.W. Sigrist, Appl. Opt. **46**, 3981 (2007)
58 S.W. Sharpe, T.J. Johnson, R.L. Sams, P.M. Chu, G.C. Rhoderick, P.A. Johnson, Appl. Spectrosc. **58**, 1452 (2004)
59 L.S. Rothman, D. Jacquemart, A. Barbe, D.C. Benner, M. Birk, L.R. Brown, M.R. Carleer, C. Chackerian Jr., K. Chance, L.H. Coudert, V. Dana, V.M. Devi, J.-M. Flaud, R.R. Gamache, A. Goldman, J.-M. Hartmann, K.W. Jucks, A.G. Macki, J.-Y. Mandin, S.T. Massie, J. Orphal, A. Perrin, C.P. Rinsland, M.A.H. Smith, R.N. Tolchenov, R.A. Toth, J. Vander Auwera, P. Varanasi, G. Wagner, J. Quantum Spectrosc. Radiat. Transf. **96**, 139 (2005)
60 L. Politi, A. Groppi, A. Polettini, J. Anal. Toxicol. **29**, 1 (2005)
61 C. Fischer, R. Bartlome, M.W. Sigrist, Appl. Phys. B **85**, 289 (2006)
62 R. Bartlome, M. Baer, M.W. Sigrist, Rev. Sci. Instrum. **78**, 013 110 (2007)
63 G. Dellepiane, J. Overend, Spectrochim. Acta **22**, 593 (1966)
64 F. Arnold, V. Burger, B. Droste-Fanke, F. Grimm, A. Krieger, J. Schneider, T. Stilp, Geophys. Res. Lett. **24**, 3017 (1997)
65 D.J. Jacob, B.-D. Field, E.M. Jin, I. Bey, L. Ainbin, J.A. Logan, R.M. Yantosca, A.B. Singh, J. Geophys. Res. D **107**, 4100 (2002)
66 F. Combes, M. Gerin, A. Wooten, G. Wlodarcak, F. Clausset, P.J. Encrenaz, Astron. Astrophys. **180**, L13 (1987)
67 L.E. Snyder, F.J. Lovas, D.M. Mehringer, N.Y. Miao, Y.-J. Kuan, J.M. Hollis, P.R. Jewell, Astrophys. J. **578**, 245 (2002)
68 D.N. Friedel, L.E. Snyder, A.J. Remijan, B.E. Turner, Astrophys J. **632**, L95 (2005)
69 C. Denga, J. Zhanga, X. Yub, W. Zhangb, X. Zhanga, J. Chromatogr. B **810**, 269 (2004)
70 H. Huang, J. Zhou, S. Chen, L. Zeng, Y. Huang, Sens. Act. B **101**, 316 (2004)

71 C. Wang, S.T. Scherrer, D. Hossain, Appl. Spectrosc. **58**, 784 (2004)
72 R. Lewicki, G. Wysocki, A.A. Kosterev, F.K. Tittel, Opt. Express **15**, 7357 (2007)
73 S. Bernegger, M.W. Sigrist, Infrared Phys. **30**, 375 (1990)
74 R.H. Mann, W.B. Dixon, J. Chem. Phys. **57**, 792 (1972)
75 K. Sato, Y. Hidaka, Combust. Flame **122**, 291 (2000)
76 R. Bartlome, J.M. Rey, M.W. Sigrist, to be published